Graph Signal Smoothness Based Feature Learning of Brain Functional Networks in Schizophrenia

Xiaoying Song, *Member, IEEE*, and Li Chai, *Member, IEEE*

***Abstract*— In this paper we study the brain functional network of schizophrenic patients based on resting-state fMRI data. Different from the region of interest (ROI)-level brain networks that describe the connectivity between brain regions, this paper constructs a subject-level brain functional network that describes the similarity between subjects from a graph signal processing (GSP) perspective. Based on the subject graph, we introduce the concept of graph signal smoothness to analyze the abnormal brain regions (feature brain regions) in which schizophrenic patients produce abnormal functional connections and to quantitatively rank the degree of abnormality of brain regions. We find that in the patients' brain networks, many new connections appear and some common connections are strengthened. The feature brain regions can be easily found according to the value of connection differences. Finally, we validate the learned feature brain regions by the results of two types of statistical analyses (ROI-to-ROI analysis and seed-to-voxel analysis), and the feature brain regions derived from graph signal smoothness are indeed the brain regions with significant differences in the statistical analysis, which illustrates the potential of graph signal smoothness for use in quantitative analysis of brain networks.**

***Index Terms*— Brain functional network, graph signal processing (GSP), graph signal smoothness, feature brain regions, schizophrenia.**

I. Introduction

SCHIZOPHRENIA is a complex mental disorder with unknown etiology that often strikes in late adolescence or early adulthood. Its diagnosis is mainly based on clinical observation of symptoms, and there is no clear biological marker for diagnosis so far [1]. Mental disorders can cause sustained and significant abnormalities in various aspects of a patient's activities, such as cognition, willpower, behavior, and emotions. Due to overlapping symptoms and a lack of standard biologically-based clinical tests, the differential diagnosis of this disease has become a challenging task [2]. In this sense, the study of brain functional network and the related biological indicators is of great significance for the research, diagnosis and treatment of the disease.

Due to the heterogeneity of schizophrenia, there may be great differences between different patients and different courses of the same patient, which brings great difficulties to the study of schizophrenia. The advancement of neuroimaging technology has enabled the measurement of human brain structure and function in a non-invasive manner [3], [4]. Among them, functional magnetic resonance imaging (fMRI) indirectly estimates brain activity at approximately every second in the form of blood oxygenation level dependent (BOLD) signals [5]. The non-invasive, repeatable and scalable nature of fMRI has made it an ideal method for investigating patterns of the function of the brain [6], [7], [8].

In the functional brain network, the brain is modelled as an undirected weighted graph, where vertices can describe atlas-based regions or voxels, and edges describe the functional connectivity of statistical relationships between the activity time series (BOLD signals) of the two vertices, and this graph structure helps enhancing our understanding of the brain as a complex system [9]. Pearson correlation, coherence and wavelet correlation are typically used to define statistical relationships between regional activity time series. This is the brain graph at the brain region of interest level (ROI-level graph). The network analysis can also be used to explore the basic principles of brain network organization and reveal the meaningful information of the topological structure of brain functional network, including small-worldness, clustering coefficient, etc [10], [11], [12], [13], [14]. Studies have found significant differences in the brain working patterns of healthy subjects and schizophrenics, and schizophrenia is increasingly being considered as a disorder or disconnection syndrome of brain networks with abnormal topological features.

Widespread abnormalities of brain regions and abnormal connections between brain regions in schizophrenic patients have been reported [15], [16], with the robust abnormal brain regions being found in the frontal lobe, parietal lobe and occipital lobe, etc. [17], [18], [19]. Specific findings include:

Manuscript received 29 March 2023; revised 11 July 2023, 14 August 2023, and 25 September 2023; accepted 25 September 2023. Date of publication 28 September 2023; date of current version 4 October 2023. This work was supported by the National Natural Science Foundation of China under Grant 62176192 and Grant 62173259. *(Corresponding author: Li Chai.)*

Xiaoying Song is with the Engineering Research Center of Metallurgical Automation and Measurement Technology, Wuhan University of Science and Technology, Wuhan 430081, China (e-mail: xiaoying811@wust.edu.cn).

Li Chai is with the State Key Laboratory of Industrial Control Technology, College of Control Science and Engineering, Zhejiang University, Hangzhou 310027, China (e-mail: chaili@zju.edu.cn).

Digital Object Identifier 10.1109/TNSRE.2023.3320135

TABLE I
ALL ABBREVIATIONS COVERED IN THE PAPER

Abbreviation	Full name	Abbreviation	Full name
ROI	region of interest	RRC	ROI-to-ROI connectivity
GSP	graph signal processing	SBC	seed-based connectivity
BOLD	blood oxygenation level dependent	DAN	dorsal attention network
fMRI	functional Magnetic Resonance Imaging	DMN	default mode network
TR	repetition time	ITG	inferior temporal gyrus
TE	echo time	LOC	lateral occipital cortex
CSF	cerebrospinal fluid	STG	superior temporal gyrus
MNI	Montreal Neurological Institute	PaHC	Para hippocampal gyrus
FWHM	full width half maximum	Cereb Crus	cerebellum crus
AAL	Automated Anatomical Labeling	FPN	frontoparietal network
RFT	random field theory		

decreased functional connectivity in the medial prefrontal cortex [20], [21], dorsal lateral prefrontal cortex [22], and orbital frontal cortex [23]; increased or decreased functional connectivity in the temporal lobe with protrusions in the left superior temporal gyrus [20], [24], etc. Other reported brain regions with functional abnormalities include left posterior cingulate, right cerebellum, parietal cortex, hippocampal, amygdala and occipital gyrus. These findings offer help in the early treatment of schizophrenia and provide the basis for understanding the pathogenesis of the disorder, yet quantitative analysis of these abnormal brain regions is lacking.

Considering brain graph as the underlying network structure, BOLD signals at each brain regions can naturally be regarded as high-dimensional signals in this graph. The emerging tools in the field of graph signal processing (GSP) are customized for dealing with such signals and are used to address issues related to analyzing and extracting information from irregular data defined in non-Euclidean spaces [25], [26], [27]. It provides a new perspective for network data processing and has great potential for applications in brain networks [28]. The basic GSP methods commonly used to analyze brain networks and signals are the graph Fourier transform (GFT) and the corresponding graph frequency components and graph filters. The fact that the GFT encodes a notion of variability similar to what the Fourier transform for temporal signals encodes is one of the GFT's key properties. The total variation of the graph signal, that is, the graph signal smoothness, has been widely used as a measure of how much the graph signal changes with respect to the network, and researchers have even defined the total variation of the eigenvectors to analyse the fluctuation of the eigenvectors on different types of connections in the brain network [28], [29]. Low and high temporal variability have proven to be important in the analysis of neurological disorders and behaviours [30], [31]. The goal of this paper is to quantitatively analyse brain functional networks using the tool of graph signal smoothness.

Different from the ROI-level graph mentioned above, this paper constructs a subject-level graph structure, referred to as the subject graph, which is a higher-level graph structure with subjects as vertices and the correlation between the subjects' BOLD signals as the edges. For each vertex, the subject's BOLD signal represents the high-dimensional signal at the vertex, and brain regions represent the feature variables. On the basis of the subject graph, we apply the tool of graph signal smoothness to learn the feature brain regions that show the greatest differences between normal subjects and schizophrenic patients, which are the predominant regions that generate abnormal connections. By quantitatively ranking the degree of abnormality in brain regions, we provide a quantitative basis for the qualitative analysis of brain networks. On the other hand, based on CONN and SPM12 toolboxes, we perform statistical analysis to infer the attributes of the control group and the patient group in the context of voxel-based and ROI-to-ROI measures. Finally, the feature brain regions learned from the graph signal smoothness are verified by the statistical analysis results.

The paper is organized as follows. Section II compares two ways to construct brain graphs. Section III presents materials used and the proposed method. Sections IV presents the applications of the proposed method in two public datasets and analyzes the feature brain regions. Sections V and VI give the discussions and conclusions on the results of the paper, respectively. All abbreviations covered in this paper are summarized in Table I.

II. TWO WAYS TO CONSTRUCT BRAIN GRAPH

A. Brain Region as Vertex

This is the most widely used method for constructing the brain graph, which describe the functional connectivities among brain regions in each subject. These connectivities are mathematically described by a weighted graph $G_1 = \{V_1, E_1, W_1\}$ where $V_1 = \{v_1, v_2, \cdots, v_N\}$ is the set of N vertices associated with specific brain regions and $W_1 \in R^{N\times N}$ is the weighted adjacency matrix. The element of W_1, w_{ij}, denotes the weight of the edge between brain regions i and j, e_{ij}. If there is no connectivity between brain regions i and j, then $w_{ij} = 0$, i.e., there is no edge between them, otherwise $w_{ij} \neq 0$. The structure of G_1 can also be described by another unweighted adjacency matrix A_1,

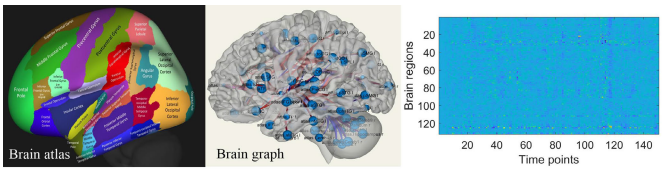

(a) Brain atlas and brain graph G_1 (b) Example brain signals of one subject

Fig. 1. Brain atlas and example brain signals.

where $a_{ij} = 1$ indicates an edge between brain regions i and j, and $a_{ij} = 0$ indicates no edge between brain regions i and j.

The brain regions encoded in the nodes of V_1 are macro-scale parcels of the brain. A variety of brain parcellation schemes exist, depending on the resolution, location of ROIs [32], [33], and the way the ROIs is defined (cytoarchitecture, anatomy, function, connectivity, etc.) [34], [35]. The larger the value of N, the higher the resolution is. A parcellation scheme including $N = 132$ ROIs is used in this paper, which will be detailed in Section III-A. The schematic diagram is shown in Fig 1(a).

For one subject, the graph signal $x_t \in R^N$ quantifies the neural activity of the entire brain at a given moment t, and its kth component x_{tk} describes the activity of the kth brain region at moment t. BOLD signals for all the N brain regions over T successive time points can be represented as $X \in R^{N\times T}$. An example of brain signal matrix for one subject is shown in Fig. 1(b).

The element w_{ij} in the weighted adjacency matrix W_1 describes the functional connectivity between region i and region j, which is usually measured by the correlation between BOLD signals on the two brain regions.

B. Subject as Vertex

In this paper, we construct the brain graph from the subject perspective, that is, subject is taken as vertex, and edges describe the correlation between subjects. In this graph $G_2 = \{V_2, E_2, W_2\}$, $V_2 = \{v_1, v_2, \cdots, v_M\}$ is the set of M vertices associated with specific subjects and $W_2 \in R^{M\times M}$ is the weighted adjacency matrix. The element of W_2, w_{ij}, denotes the weight of the correlation between subjects i and j, e_{ij}. If there is no correlation between subjects i and j, or the absolute value of the correlation is less than a preset threshold, then $w_{ij} = 0$, i.e., there is no edge between them, otherwise $w_{ij} \neq 0$. The unweighted structure of G_2 can be described by A_2, which is defined in the same way as A_1.

Taking the $N = 132$ brain regions as feature variables, the construction method of graph signal on subject graph G_2 is shown in Fig. 2. In the setting of graph G_2, the original signal on each vertex (subject) is a signal matrix consisting of BOLD time series from all brain regions. In order to adopt graph signal processing approaches it is necessary to dimensionally reduce this signal matrix into a column vector, i.e. a high-dimensional signal on each vertex (instead of a signal matrix), and this operation also enables each feature variable to be a real number (instead of a vector).

A common method of dimensionality reduction is to average the BOLD signals over each brain region [29], and in this paper we use the power of the BOLD time series over

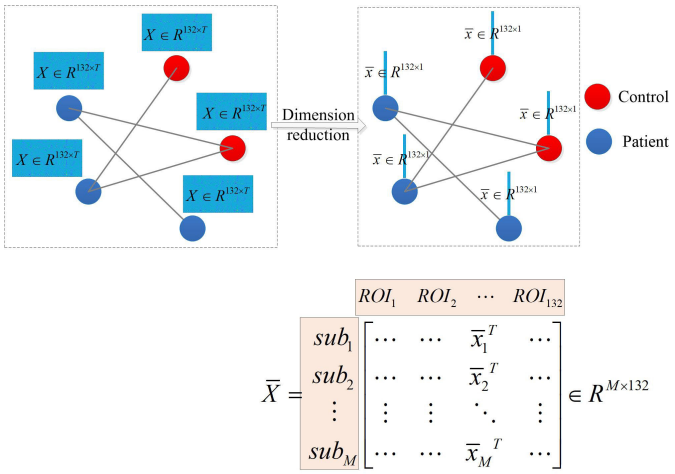

Fig. 2. Dimension reduction of data on an example subject graph G_2 (there are 5 subjects, of which 3 are patients and 2 are healthy subjects).

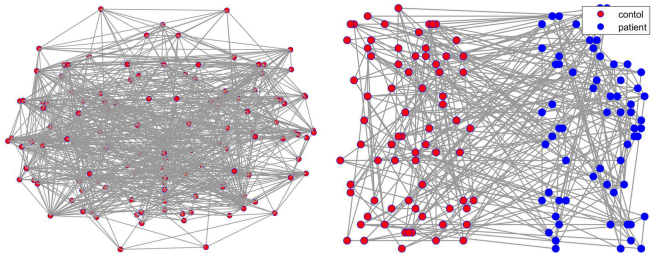

(a) Anterior brain view (N=132 ROIs) (b) Subject graph (N=145 subjects)

Fig. 3. For the COBRE dataset used in experiments, the comparison of these two graphs.

each brain region to obtain more accurate information. Let $X_k = [X_{k1}, X_{k2}, \cdots, X_{kT}] \in R^{1\times T}$, $k \in \mathcal{N} = \{1, 2, \cdots, N\}$ be the kth row of X, that is, the BOLD time series on the kth brain region. The average power of this time series over a length time of T is $\bar{x}_{(k)} = \frac{1}{T}\sum_{t=1}^{T} |X_{kt}|^2$. Then, we get a high-dimensional signal $\bar{x} = [\bar{x}_{(1)}, \cdots, \bar{x}_{(k)}, \cdots, \bar{x}_{(N)}]^T \in R^N$ for each subject.

Signal matrix $\bar{X} = [\bar{x}_1, \cdots, \bar{x}_i, \cdots, \bar{x}_M]^T$ collects all high-dimensional signals $\bar{x}_i$'s in its M rows, and its kth column, $\bar{X}_k$, describes the graph signal of all subjects on the kth brain region.

For the COBRE dataset used in the following experiments, the comparison of these two graphs are shown in Fig. 3.

III. Materials and Methods

A. Data and Preprocessing

Two public datasets on schizophrenia are used in this paper. COBRE dataset[1] from NITRC contains 72 patients with schizophrenia and 75 healthy subjects. Due to the length of volumes is not consistent with the others, two subjects are deleted. In the end, 71 patients with schizophrenia (patient group) and 74 healthy subjects (control group) are analyzed for this dataset. The resting-state fMRI images are obtained with the following parameters: TR (repetition time) = 2000 ms, TE (echo time) = 29 ms,

[1] http://fcon_1000.projects.nitrc.org/indi/retro/cobre.html

TABLE II
SUBJECT INFORMATION FOR TWO DATASETS

	Clinic Cohort	Number	Age (mean±std)	Gender (male/female)
COBRE	Patient	71	38±13.72	57/14
	Control	74	35±11.74	51/23
OpenNEURO	Patient	49	36±8.79	37/12
	Control	117	31±8.70	62/55

matrix size = 64 × 64, flip angle = 77°, voxel size = $3 \times 3 \times 4\ mm^3$, T = 150 volumes.

OpenNEURO dataset [36], [37] is obtained from the OpenfMRI database, which is a large study funded by the UCLA Consortium for Neuropsychiatric Phenomics LA5c Study. This dataset contains three types of diseases, of which only 49 patients with schizophrenia and 117 healthy subjects are analyzed in our experiments. The resting-state fMRI images are obtained with the following parameters: TR (repetition time) = 2000 ms, TE (echo time) = 30 ms, matrix size = 64 × 64, T = 152 volumes.

Table II shows the information of subjects for these two datasets. For these two datasets, the resting-state fMRI data are used in this paper. In the resting scan, participants are asked to remain relaxed and keep their eyes open for 5 minutes (COBRE) and 5 minutes and 4 seconds (OpenNEURO). They are not presented any stimuli or asked to respond during the scan.

Resting-state fMRI data of all subjects are preprocessed according to the standard preprocessing pipeline provided by the CONN[2] and SPM12[3] toolboxes, including: realignment and unwarp (subject motion estimation and correction), slice-timing correction (correction for inter-slice differences in acquisition time), outlier detection (identification of outlier scans for scrubbing), segmentation and normalization (simultaneous grey/white/CSF segmentation and Montreal Neurological Institute (MNI) normalization), spatially smoothing (Gaussian kernel of 8 mm full width half maximum (FWHM)), etc. After these conventional preprocessing steps, the influence of potential confounding effects in the measured BOLD signal is linear regressed out. These noises come from the combination of physiological effects (white matter and CSF), outliers, and residual subject-motion factors (12 parameters).

According to the CONN's built-in *atlas* template, a total of $N = 132$ non-overlapping ROIs are mapped to cover the whole brain. Among which, 91 Cortical regions are derived from the FSL Harvard-Oxford Atlas maximum likelihood cortical atlas and are divided into left/right hemisphere (91 ROIs); 15 subcortical regions are derived from the FSL Harvard-Oxford Atlas maximum likelihood subcortical atlas, ignoring the Cerebral White Matter, Cerebral Cortex and Lateral Ventrical areas (15 ROIs); 26 cerebellar regions are derived from the Automated Anatomical Labeling (AAL) Atlas (26 ROIs). The signal matrix $X \in R^{N \times T}$ describes the signals on all ROIs of each subject. For COBRE and OpenNEURO dataset, the signal matrix is $X \in R^{132 \times 150}$ and $X \in R^{132 \times 152}$, respectively.

[2]version 20b, https://www.nitrc.org/projects/conn
[3]http://www.fil.ion.ucl.ac.uk/spm/

B. Feature ROIs Learning

Given a brain graph $G = \{V, E, W\}$, no matter which way it is constructed, conventional degree and Laplacian matrices are used [38]. The degree matrix is defined as $D := diag(d_i)$, where $d_i = \sum_j a_{ij}$ is the degree of the vertex v_i. The Laplacian matrix can be defined as $L = D - A$, which is a real symmetric semi-positive definite matrix that can be decomposed using eigenvalues,

$$L = V \Lambda V^{-1}. \tag{1}$$

The eigenvector matrix is defined as $V := [v_1, v_2, \cdots, v_N]$. The diagonal eigenvalue matrix is defined as $\Lambda := diag(\lambda_1, \lambda_2, \cdots, \lambda_N)$ and its eigenvalues $\{0 \leq \lambda_1 \leq \lambda_2 \cdots \leq \lambda_N\}$ are defined as the spectrum of the graph. The spectrum carries a specific notion of frequency, with the eigenvectors associated with higher eigenvalues fluctuate more rapidly (high frequency).

Given a graph signal y (x_t or $\bar{X}_k$ we state above), according to the 2-Dirichlet form of y, its global smoothness relative to the intrinsic structure of the graph G can be defined as

$$\phi(y) = y^T L y = \sum_{(i,j) \in E} a_{i,j}[y(j) - y(i)]^2. \tag{2}$$

The global smoothness is a measure of how much the graph signal y changes with respect to the graph. Given the structure of the graph, then the adjacency matrices W and A are determined, the smaller the value of $\phi(y)$, the slower the signal changes with respect to the graph and the more low-frequency components of the signal, that is, the smoother the signal y. The signal y is more likely to be smooth when the values of the signal y at the connected vertices are similar, or when two vertices with very different values of the signal y are not connected. We also notice that $\phi(y)$ is equal to zero if and only if y is constant across all vertices (the boundary case of completely non-connected graphs is not considered).

In the setting of the subject graph G_2, brain regions represent the feature variables on each vertex, with $N = 132$ ROIs (features) per vertex. For the graph signal $\bar{X}_k$, the corresponding $\phi(\bar{X}_k)$ characterizes the similarity of activity on the kth brain region for all subjects. Based on subjects' performance on all ROIs, we can explore those brain regions that differ most between healthy subjects and patients, and these abnormal brain regions (referred to here as the feature ROIs) give rise to abnormal connectivities in the patient's functional brain network. We construct the weighted adjacency matrix W_2 of G_2 based on the Pearson correlation between subjects. If the Pearson correlation coefficient is less than a given threshold, the two subjects are considered unrelated. The larger the threshold, the sparser the structure of G_2.

Let the Laplacian matrix of G_2 be L_2, and for simplicity, the smoothness of the signal matrix $\bar{X}$ can be defined as

$$\Phi = tr(\bar{X}^T L_2 \bar{X}), \tag{3}$$

where $\Phi = \{\phi_1, \phi_2, \cdots, \phi_k, \cdots, \phi_{132}\}$, and ϕ_k describes the smoothness of signals of all subjects on the kth brain region (ROI_k).

Larger ϕ_k values indicate that patients and healthy subjects show a large difference in ROI_k, and this region can be regarded as a feature brain region. Conversely, a small ϕ_k value indicates that patients and healthy subjects show similar performance on ROI_k, and this region can be regarded as a non-feature brain region. To remove the effect of within-group variance on the results, separate networks G_c and G_p are constructed for the control and patient groups, based on which Φ_c and Φ_p are calculated and subtracted from Φ as the within-group variance to obtain the final

$$\tilde{\Phi} = \Phi - \Phi_c - \Phi_p. \tag{4}$$

Sorting $\tilde{\Phi} = \{\tilde{\phi}_1, \tilde{\phi}_2, \cdots, \tilde{\phi}_k, \cdots, \tilde{\phi}_{132}\}$ in descending order, we can focus on the top few most important brain regions and the least important ones. Furthermore, we can set a threshold T_ϕ for the ranked $\tilde{\Phi}$. The top k ranked brain areas with $\tilde{\phi}_k > T_\phi$ are considered feature brain regions, whereas the other $(132 - k)$ brain regions at the bottom of the ranking are considered non-feature brain regions.

C. Statistical Analysis

To validate the learned feature brain regions derived from graph signal smoothness, we quantify the level of functional integration in different brain regions from two aspects: 1) seed-to-voxel analysis, which aims to investigate the functional connectivity properties of individual regions; 2) ROI-to-ROI analysis, which aims to analyze connectivity patterns among multiple regions.

The seed-to-voxel analysis uses seed-based connectivity (SBC) maps to represent the level of functional connectivity between a seed ROI and each voxel in the brain, calculated as the Fisher transform of the Pearson correlation coefficients between the BOLD time series of the seed ROI and voxels. Similar to the voxel-based analysis, we also investigate the entire connectivity network of the brain using the ROI-to-ROI analysis, which characterizes the level of functional connectivity between all passible pairwise ROIs with ROI-to-ROI connectivity (RRC) matrices, defined as the Fisher transform of the bivariate correlation coefficient between pairs of ROI BOLD time series.

Further, instead of focusing on individual voxels, we analyze the functional connectivity differences between the control and the patient groups on a cluster level based on statistical tests (t-test or F-test) to make more meaningful inferences. Using the standard general linear model analysis for the SBC connectivity map, we analyze the clustering of the connections of the two groups based on the generated statistical parametric maps (corresponding T- or F- values). We define clusters using Gaussian Random Field Theory (RFT) parametric statistics [39]. This standard employs a combination of RFT and an uncorrected height threshold of $p < 0.001$ to define clusters of interest from the original statistical parametric maps, and selects those considered to be significant in the resulting clusters using a FDR-corrected cluster-level threshold of $p < 0.05$. The characteristic of each cluster is determined by its size, measured in the number of voxels, and the uncorrected p-value of clusters deemed significant is $p < 0.001$.

Similar to the voxel-based analysis scenario, when there are many ROIs, it is frequently more convenient to focus on clusters of close or related connections that share comparable effects rather than on individual connections between every conceivable pair of ROIs. Applying multivariate parametric statistics based on functional network connectivity [40], we analyze the entire set of connections between ROIs, both from the perspective of within and between clusters of connections. The standard employs a FDR-corrected cluster-level threshold of $p < 0.05$ to select significant connection sets from all group-to-group connection sets, and characterizes the patterns of individual connections that show the largest effects within each significant set using a post-hoc uncorrected height threshold of $p < 0.05$. The criterion uses a FDR-corrected $p < 0.05$ cluster-level threshold to select among all group-to-group connectivity sets those deemed significant, together with a post-hoc uncorrected $p < 0.05$ height (connection-level) threshold to help characterize the pattern of individual connections that show some of the largest effects within each significant set.

IV. Results

A. Feature ROIs

We set a two-sided threshold to ensure that the subject graph G_2 has the same connection density during quantitative and qualitative analysis.

For the COBRE dataset, we find that the most important brain regions are: ROI_28, ROI_27, ROI_69, ROI_124, ROI_68, ROI_90, ROI_91, ROI_30, ROI_123, ROI_29, ROI_125, ROI_63, ROI_62. The least important brain regions include: ROI_13, ROI_14, ROI_96, ROI_97, ROI_98, ROI_99, ROI_54, ROI_78, ROI_79, ROI_55.

For the OpenNEURO dataset, we find that the most important brain regions are: ROI_27, ROI_69, ROI_28, ROI_68, ROI_125, ROI_123, ROI_124, ROI_62, ROI_63, ROI_30, ROI_29, ROI_132. The least important brain regions include: ROI_76, ROI_77, ROI_14, ROI_13, ROI_97, ROI_96, ROI_54, ROI_78, ROI_79, ROI_53.

Taken together, these findings indicate that the most important feature ROIs are consistent on both datasets. Based on the above results, for schizophrenic patients, we can draw the following conclusions:

1) ROI_27-30 (inferior temporal gyrus), ROI_68-69 (temporal fusiform cortex), ROI_124-125 (cerebelum 10 (right), vermis (1 and 2)), and ROI_62-63 (parahippocampal gyrus) are the main areas with abnormal connections.

2) Brain regions such as ROI_13-14 (precentral gyrus), ROI_96-97 (putamen) and ROI_78-79 (central opercular cortex) have little impairment in function.

B. Seed-to-Voxel Analysis Results

The results of the statistical analyses are basically the same for both the COBRE and openNEURO datasets, similar to the results of the numerical calculations above. Only the results

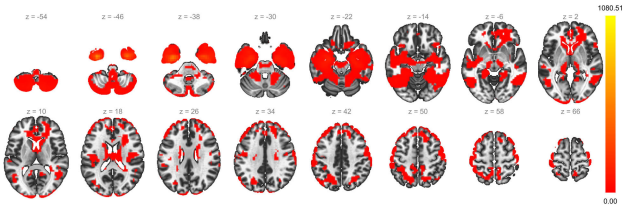

(a) the control group

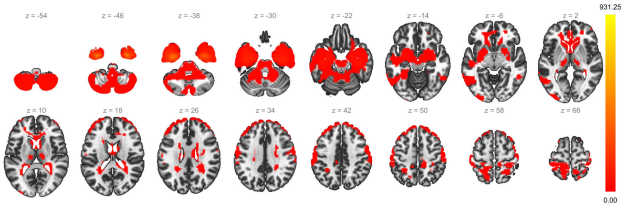

(b) the patient group

Fig. 4. The SBC maps with two temporal fusiform cortex seeds of control and patient groups.

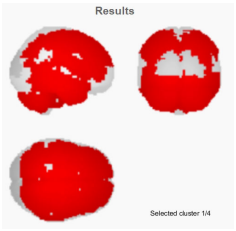

(a) the control group

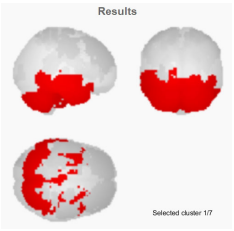

(b) the patient group

Fig. 5. The RFT cluster-level inferences of the temporal fusiform cortex of control and patient groups.

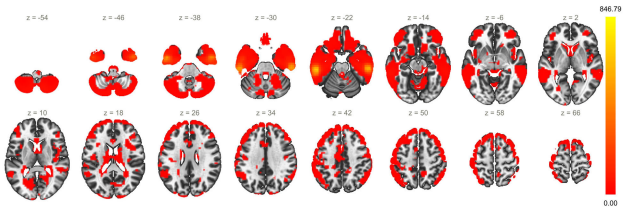

(a) the control group

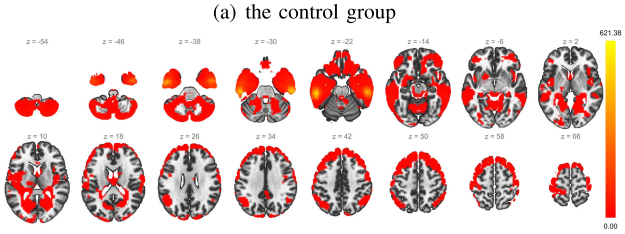

(b) the patient group

Fig. 6. The SBC maps with four inferior temporal gyrus seeds of control and patient groups.

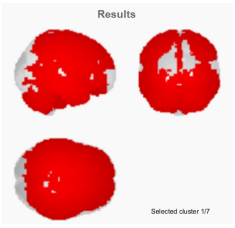

(a) the control group

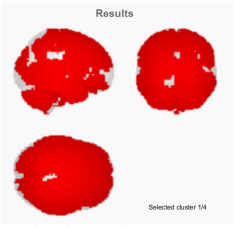

(b) the patient group

Fig. 7. The RFT cluster-level inferences of the inferior temporal gyrus of control and patient groups.

from the COBRE dataset are analysed due to the length of the paper.

1) Temporal Fusiform Cortex: Taking the anterior right (ROI_68, $\tilde{\phi}_{68} = 4453.37$) and anterior left (ROI_69, $\tilde{\phi}_{69} = 5801.63$) division of the temporal fusiform cortex as seed regions, we use seed-based analysis to analyze functional connectivity levels between these two seeds and each voxel in the brain.

The average SBC map with these two seeds across 71 patients and 74 healthy subjects are shown in Fig. 4(a) and Fig. 4(b), respectively. The connectivity pattern of one seed ROI usually includes this region. Comparing figures 4(a) and 4(b), we can see that the control group has a stronger level of connectivity homogeneity across the temporal fusiform cortex. In addition, the connectivity pattern of the control group includes more distant regions, indicating that the temporal fusiform cortex of the control group has stronger strength of inter-regional connectivity.

The report of RFT cluster-level inferences for the temporal fusiform cortex of control and patient groups are shown in Fig. 5(a) and Fig. 5(b), respectively. The control group has four significant activation clusters, the largest of which contains 65167 voxels, while the patient group has seven significant clusters, and the largest of which contains 37082 voxels.

2) Inferior Temporal Gyrus: Taking the anterior right (ROI_27, $\tilde{\phi}_{27} = 12217.05$), anterior left (ROI_28, $\tilde{\phi}_{28} = 17745.50$), posterior right (ROI_29, $\tilde{\phi}_{29} = 848.80$), and posterior left (ROI_30, $\tilde{\phi}_{30} = 1517.62$) division of the inferior temporal gyrus as seed regions, we exactly use the same SBC map and RFT parametric statistics to analyze functional connectivity levels between these four seeds and each voxel in the brain. The comparison of results between control and patient groups are shown in Fig. 6 and Fig. 7.

The control group has a stronger level of connectivity homogeneity across the inferior temporal gyrus. The control group has more significant activation clusters. The number of voxels contained within the largest cluster is basically the same for the control and patient groups, 81020 and 84740, respectively.

3) Parahippocampal Gyrus: Taking the anterior right (ROI_62, $\tilde{\phi}_{62} = 703.75$) and anterior left (ROI_63, $\tilde{\phi}_{63} = 942.32$) division of the parahippocampal gyrus as seed regions, we adopt SBC map and RFT parametric statistics to analyze functional connectivity levels between these two seeds and each voxel in the brain. The comparison of results between control and patient groups are shown in Fig. 8 and Fig. 9.

The patient group has a stronger level of connectivity homogeneity across the parahippocampal gyrus. The patient group has more significant activation clusters. The largest cluster for the control group contains 63514 voxels, whereas the largest cluster for the patient group contains 44075 voxels.

4) Precentral Gyrus: Taking the right (ROI_13, $\tilde{\phi}_{13} = 4.44$) and left (ROI_14, $\tilde{\phi}_{14} = 4.15$) division of the precentral gyrus as seed regions, we adopt SBC map and RFT parametric statistics to analyze functional connectivity levels between these two seeds and each voxel in the brain. The comparison

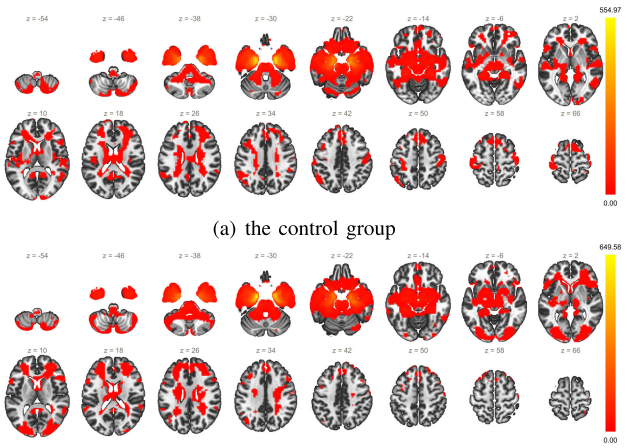

(a) the control group

(b) the patient group

Fig. 8. The SBC maps with two parahippocampal gyrus seeds of control and patient groups.

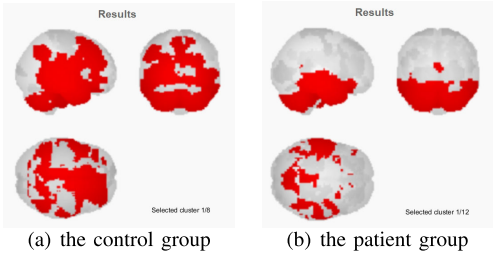

(a) the control group (b) the patient group

Fig. 9. The report of RFT cluster level inferences of the parahippocampal gyrus of control and patient groups.

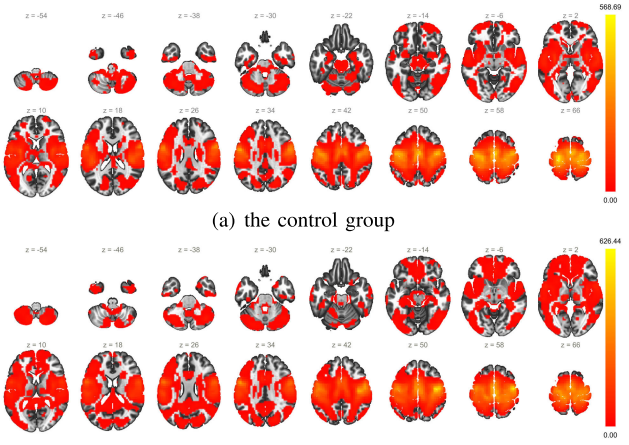

(a) the control group

(b) the patient group

Fig. 10. The SBC maps with two precentral gyrus seeds of control and patient groups.

of results between control and patient groups are shown in Fig. 10 and Fig. 11.

In numerical calculations, there are no significant differences between the control and patient groups in these two brain regions, which are considered to be non-feature brain regions. Seed-to-voxel analysis reveals only two significant activation clusters in both groups, and both clusters contain a comparable number of voxels (larger cluster: 118089 vs. 128845, smaller cluster: 303 vs. 707), suggesting that the control and patient groups are performing almost identically in these two brain

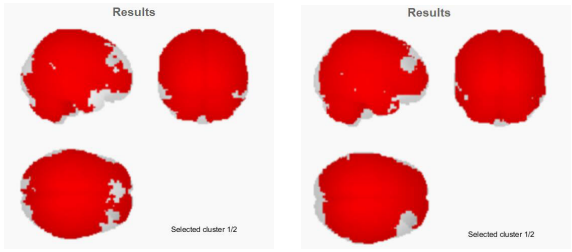

(a) the control group (b) the patient group

Fig. 11. The report of RFT cluster level inferences of the precentral gyrus of control and patient groups.

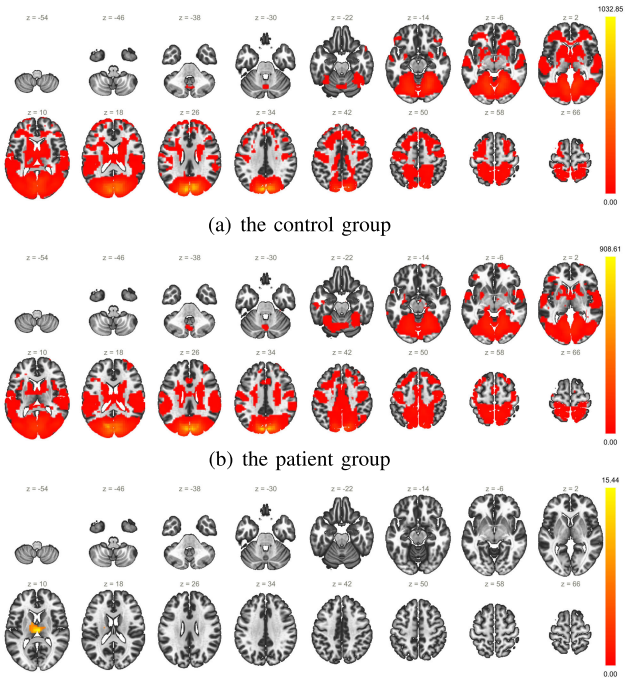

(a) the control group

(b) the patient group

(c) patient-control

Fig. 12. The SBC maps with two cuneal cortex seeds of control and patient groups.

regions. Thus, the statistical results confirm the validity of the numerical results calculated from graph signal smoothness.

5) Cuneal Cortex: In order to determine a suitable threshold T_ϕ for the sorted $\tilde{\Phi}$ to find out all the abnormal brain regions, we select two seed regions with smoothness $\tilde{\Phi}$ sorted between 60 and 70 (close to 50% of 132): ROI_58 (the right division of the cuneal cortex, $\tilde{\phi}_{58} = 34.40$) and ROI_59 (the left division of the cuneal cortex, $\tilde{\phi}_{59} = 23.74$), and analyze the SBC maps of the control group and the patient group based on these two seed regions, and the results are shown in Fig. 12. We can observe that the largest cluster in the control group has 78663 voxels and covers 86% of the precuneus cortex, 56% of the lateral occipital cortex (superior division right), 50% of the lateral occipital cortex (superior division left), and other regions. Similar to the control group, the largest clusters in the patient group has 77158 voxels and covers 97% of the precuneus cortex, 78% of the lateral occipital cortex (superior division right), 56% of the lateral occipital cortex (superior division left), and other regions.

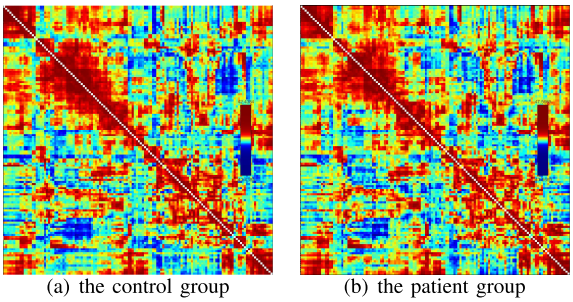

(a) the control group (b) the patient group

Fig. 13. Average RRC matrix of control and patient groups.

We also show the difference map for the two groups (patient-control) in Fig. 12(c). There is only one cluster in the difference map, which has only 606 voxels and mainly covers the thalamus. Considering the small number and size of the cluster in the difference map, it is feasible to take the threshold $T_\phi = \tilde{\phi}_{58}$, i.e., the brain regions with a smoothness ranking in the top 62 (the ranking of ROI_58) can all be regarded as feature brain regions, and all the brain regions ranked after 63 can naturally be regarded as non-featured brain regions. Of course, based on the SBC analysis, we can further increase the value of T_ϕ to reduce the number of feature brain regions.

C. ROI-to-ROI Analysis Results

The average 132-ROIs RRC matrix across 71 patients and 74 healthy subjects are shown in Fig. 13(a) and Fig. 13(b), respectively.

For *atlas* $N = 132$, there are a maximum of 8646 connections, and the 132 ROIs are grouped into 22 clusters using a priori order of the CONN atlas. We perform the analysis using multivariate parametric statistics, and the results of the cluster-level inference of functional network connectivity between the patient and control groups (patient-control) are shown in Fig. 14(a), and the corresponding RRC matrix is shown in Fig. 14(b). Compared with healthy people, we derive the following cluster-based inferences for patients with schizophrenia.

1) The Thalamus group shows increased/strengthened connectivity with pDMN, IDMN, sLOC, DAN, Visual. Primary, Visual. Secondary, Motor, Auditory, STG, and Cerebellum/pPaHC groups, and decreased/weakened connectivity with Cereb Crus and FPN groups.

2) The Lang(R) group shows decreased/weakened connectivity with Limbic/aPaHC, Salience, and Auditory groups, and increased/strengthened connectivity with Motor, DAN, and sLOC groups.

3) The connections between DAN, cerebellum/pPaHC, Cereb Crus, Cerebellum (ROI_124), and Visual groups are increased/strengthened.

4) The change of the connection between the Salience group and other groups is complex. In multiple groups, such as STG, Limbic/aPaHC and IDMN, there are both increased and decreased connections.

5) The Autitory group shows decreased/weakened connectivity with STG, Limbic/aPaHC, aDMN, and Lang(R) groups.

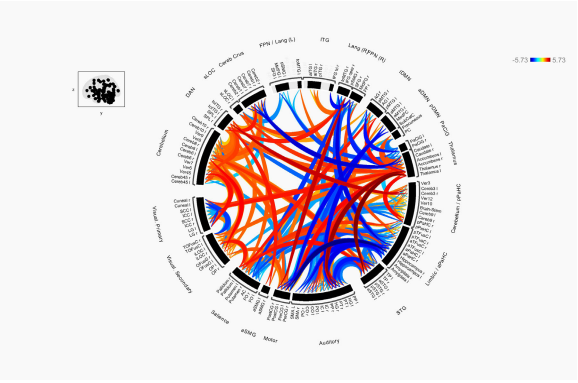

(a) functional network connectivity (22 clusters)

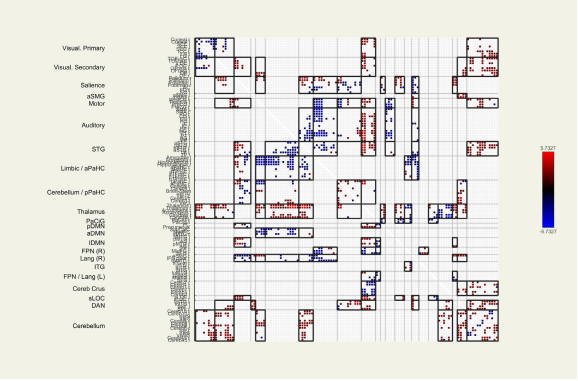

(b) RRC matrix

Fig. 14. The functional network connectivity and the corresponding RRC matrix of the difference between patient and control groups (patient-control).

6) The Limbic/aPaHC (ROI_68, ROI_69, ROI_62, ROI_63, ROI_125) group shows decreased/weakened connectivity with Lang(R), FPN(R), Auditory, Motor, Salience, and STG groups, with the largest reduction in connectivity with Motor.

7) The ITG (ROI_27, ROI_28, ROI_29, ROI_30) group shows increased/strengthened connectivity with the FPN (R) group.

Overall, patients have more increased/strengthened connections than decreased/weakened connections in the brain networks. The numerical calculation results are generally consistent with the statistical analysis results in CONN, verifying the effectiveness of the graph signal smoothness based method.

V. Discussion

Schizophrenia is a comprehensive mental disease, which contains a variety of symptoms and subtypes. There are still many difficulties in clinical research and treatment. Its etiology is very complex, and there is no clear conclusion so far. The study of brain functional network can provide a powerful target for clinical diagnosis to a certain extent. The brain's functions stem from the functional connectivity of statistical relationships between the BOLD signals of brain regions, and the highly complex structure and functions of the brain are the main focus of research [41], [42]. Developments in neuroscience have identified key roles for certain connections in the development of positive, negative, and cognitive symptoms, particularly those involving frontal, temporal, and mesostriatal brain regions.

The development of graph theory provides the basis and analytical methods for brain network research [43]. The emergence of the combination of network neuroscience and graph theory helps us better understand the relevance between network structure and cognitive function. In recent years, brain network research combined with graph theory [12], [13] have been developed to study the functional connection between multiple brain regions.

Schizophrenia has been investigated by comparable approaches. In addition to the graph Fourier transform and graph filtering, which are often used to analyze brain networks, this paper introduces another graph signal processing tool, graph signal smoothness, to learn the abnormal brain regions and abnormal connections between brain regions, and attempt to rank the importance of abnormal brain regions. The feature brain regions learnt from the graph signal smoothness are verified in the statistical analysis results in the context of voxel-based and ROI-to-ROI measures.

In the following, we discuss our results with those of existing neural and medical studies on schizophrenia. The feature brain regions ROI_27-30 (inferior temporal gyrus) and ROI_68-69 (temporal fusiform cortex) have been widely reported by existing work [15], [16], [17], [19], [20], [24]. The feature brain regions ROI_124-125 (cerebelum 10 (right), vermis (1 and 2), $\tilde{\phi}_{124} = 6187.81$, $\tilde{\phi}_{125} = 819.36$) have been reported by many work [16], [17], [18]. The feature brain regions ROI_62-63 (parahippocampal gyrus) have also been reported in [15]. All the above 10 feature brain regions reported in literature are within the top 17 feature regions according to the ranking of graph signal smoothness with $\tilde{\phi} \in [500, 17745.50]$. It is reasonable to believe that the other 7 regions not reported in literature are also important for schizophrenia research. There are 20 regions with $\tilde{\phi}$ between 100 and 500, which we regard as secondary feature regions, and it is also reasonable to believe that these brain regions should be considered in future research as potential abnormal regions of schizophrenia patients. The remaining 95 regions have $\tilde{\phi}$ values less than 100, which is very small compared to the $\tilde{\phi}$ values of the feature brain regions, so it is reasonable to treat them as non-feature brain regions. In this sense, the proposed method can be used to discover new feature brain regions and non-feature brain regions, which has great potential application as AI-assisted research of schizophrenia.

VI. Conclusion

We have applied the tool of graph signal smoothness to analyze functional brain networks of patients with schizophrenia during resting state and have established the subject graph to learn the feature brain regions. The results have shown that the numerical results calculated based on the graph signal smoothness are generally consistent with the results of the statistical analyses, and the featured brain regions learnt in this paper are also in agreement with the findings of the existing work, which proves the potential value of the application of the graph signal smoothness for quantitative analyses in the field of brain sciences.

References

[1] P. Tyrer, "A comparison of DSM and ICD classifications of mental disorder," *Adv. Psychiatric Treatment*, vol. 20, no. 4, pp. 280–285, Jul. 2014.

[2] M. R. Arbabshirani, K. A. Kiehl, G. D. Pearlson, and V. D. Calhoun, "Classification of schizophrenia patients based on resting-state functional network connectivity," *Frontiers Neurosci.*, vol. 7, p. 133, Jul. 2013.

[3] M. Mather, J. T. Cacioppo, and N. Kanwisher, "Introduction to the special section: 20 years of fMRI—What has it done for understanding cognition?" *Perspect. Psychol. Sci.*, vol. 8, no. 1, pp. 41–43, Jan. 2013.

[4] R. Hu et al., "Multi-band brain network analysis for functional neuroimaging biomarker identification," *IEEE Trans. Med. Imag.*, vol. 40, no. 12, pp. 3843–3855, Dec. 2021.

[5] Y. Bai et al., "A joint analysis of multi-paradigm fMRI data with its application to cognitive study," *IEEE Trans. Med. Imag.*, vol. 40, no. 3, pp. 951–962, Mar. 2021.

[6] L.-D. Lord, P. Expert, J. F. Huckins, and F. E. Turkheimer, "Cerebral energy metabolism and the brain's functional network architecture: An integrative review," *J. Cerebral Blood Flow Metabolism*, vol. 33, no. 9, pp. 1347–1354, Sep. 2013.

[7] Y. Liang, B. Liu, and H. Zhang, "A convolutional neural network combined with prototype learning framework for brain functional network classification of autism spectrum disorder," *IEEE Trans. Neural Syst. Rehabil. Eng.*, vol. 29, pp. 2193–2202, 2021.

[8] D. Jin, R. Li, and J. Xu, "Multiscale community detection in functional brain networks constructed using dynamic time warping," *IEEE Trans. Neural Syst. Rehabil. Eng.*, vol. 28, no. 1, pp. 52–61, Jan. 2020.

[9] D. M. A. Mehler and K. P. Kording, "The lure of misleading causal statements in functional connectivity research," 2018, *arXiv:1812.03363*.

[10] T. E. Mwansisya et al., "Task and resting-state fMRI studies in first-episode schizophrenia: A systematic review," *Schizophrenia Res.*, vol. 189, pp. 9–18, Nov. 2017.

[11] Z. Yao, B. Hu, Y. Xie, P. Moore, and J. Zheng, "A review of structural and functional brain networks: Small world and atlas," *Brain Informat.*, vol. 2, no. 1, pp. 45–52, Mar. 2015.

[12] E. Bullmore and O. Sporns, "Complex brain networks: Graph theoretical analysis of structural and functional systems," *Nature Rev. Neurosci.*, vol. 10, no. 3, pp. 186–198, Mar. 2009.

[13] M. Rubinov and O. Sporns, "Complex network measures of brain connectivity: Uses and interpretations," *Neuroimage*, vol. 52, no. 3, pp. 1059–1069, Sep. 2010.

[14] S. Ren et al., "Dynamic functional segregation and integration in human brain network during complex tasks," *IEEE Trans. Neural Syst. Rehabil. Eng.*, vol. 25, no. 6, pp. 547–556, Jun. 2017.

[15] K. H. Karlsgodt, D. Sun, and T. D. Cannon, "Structural and functional brain abnormalities in schizophrenia," *Current Directions Psychol. Sci.*, vol. 19, no. 4, pp. 226–231, Aug. 2010.

[16] V. D. Calhoun, "Functional brain networks in schizophrenia: A review," *Frontiers Human Neurosci.*, vol. 3, p. 17, Aug. 2009.

[17] T. Moberget et al., "Cerebellar volume and cerebellocerebral structural covariance in schizophrenia: A multisite mega-analysis of 983 patients and 1349 healthy controls," *Mol. Psychiatry*, vol. 23, no. 6, pp. 1512–1520, Jun. 2018.

[18] W. Lei et al., "Sex-specific patterns of aberrant brain function in first-episode treatment-naive patients with schizophrenia," *Int. J. Mol. Sci.*, vol. 16, no. 7, pp. 16125–16143, Jul. 2015.

[19] M. P. van den Heuvel, R. C. W. Mandl, C. J. Stam, R. S. Kahn, and H. E. H. Pol, "Aberrant frontal and temporal complex network structure in schizophrenia: A graph theoretical analysis," *J. Neurosci.*, vol. 30, no. 47, pp. 15915–15926, Nov. 2010.

[20] W. Guo et al., "Abnormal default-mode network homogeneity in first-episode, drug-naive schizophrenia at rest," *Prog. Neuro-Psychopharmacol. Biol. Psychiatry*, vol. 49, pp. 16–20, Mar. 2014.

[21] X.-Q. Huang et al., "Localization of cerebral functional deficits in treatment-naive, first-episode schizophrenia using resting-state fMRI," *Neuroimage*, vol. 49, no. 4, pp. 2901–2906, Feb. 2010.

[22] Y. Zhou et al., "Functional dysconnectivity of the dorsolateral prefrontal cortex in first-episode schizophrenia using resting-state fMRI," *Neurosci. Lett.*, vol. 417, no. 3, pp. 297–302, May 2007.

[23] Z. He et al., "Aberrant intrinsic brain activity and cognitive deficit in first-episode treatment-naive patients with schizophrenia," *Psychol. Med.*, vol. 43, no. 4, pp. 769–780, Apr. 2013.

[24] S. Lui et al., "Short-term effects of antipsychotic treatment on cerebral function in drug-naive first-episode schizophrenia revealed by 'resting state' functional magnetic resonance imaging," *Arch. Gen. Psychiatry*, vol. 67, no. 8, pp. 783–792, 2010.

[25] A. Sandryhaila and J. M. F. Moura, "Discrete signal processing on graphs," *IEEE Trans. Signal Process.*, vol. 61, no. 7, pp. 1644–1656, Apr. 2013.

[26] D. I. Shuman, S. K. Narang, P. Frossard, A. Ortega, and P. Vandergheynst, "The emerging field of signal processing on graphs: Extending high-dimensional data analysis to networks and other irregular domains," *IEEE Signal Process. Mag.*, vol. 30, no. 3, pp. 83–98, May 2013.

[27] A. Ortega, P. Frossard, J. Kovačević, J. M. Moura, and P. Vandergheynst, "Graph signal processing: Overview, challenges, and applications," *Proc. IEEE*, vol. 106, no. 5, pp. 808–828, May 2018.

[28] W. Huang et al., "A graph signal processing perspective on functional brain imaging," *Proc. IEEE*, vol. 106, no. 5, pp. 868–885, May 2018.

[29] W. Huang et al., "Graph frequency analysis of brain signals," *IEEE J. Sel. Topics Signal Process.*, vol. 10, no. 7, pp. 1189–1203, Oct. 2016.

[30] D. D. Garrett, N. Kovacevic, A. R. McIntosh, and C. L. Grady, "The modulation of BOLD variability between cognitive states varies by age and processing speed," *Cerebral Cortex*, vol. 23, no. 3, pp. 684–693, Mar. 2013.

[31] J. J. Heisz, J. M. Shedden, and A. R. McIntosh, "Relating brain signal variability to knowledge representation," *Neuroimage*, vol. 63, no. 3, pp. 1384–1392, Nov. 2012.

[32] A. Zalesky et al., "Whole-brain anatomical networks: Does the choice of nodes matter?" *Neuroimage*, vol. 50, no. 3, pp. 970–983, Apr. 2010.

[33] O. Sporns, *Networks of the Brain*. Cambridge, MA, USA: MIT Press, 2016.

[34] S. B. Eickhoff, B. T. T. Yeo, and S. Genon, "Imaging-based parcellations of the human brain," *Nature Rev. Neurosci.*, vol. 19, no. 11, pp. 672–686, Nov. 2018.

[35] O. Korhonen, M. Zanin, and D. Papo, "Principles and open questions in functional brain network reconstruction," *Human Brain Mapping*, vol. 42, no. 11, pp. 3680–3711, Aug. 2021.

[36] R. Bilder et al., "UCLA consortium for neuropsychiatric phenomics LA5c study," Stanford Digit. Repository, 2016. [Online]. Available: http://purl.stanford.edu/mg599hw5271 and https://openfmri.org/dataset/ds000030/

[37] R. A. Poldrack et al., "A phenome-wide examination of neural and cognitive function," *Sci. Data*, vol. 3, no. 1, pp. 1–12, Dec. 2016.

[38] F. R. Chung, *Spectral Graph Theory*, vol. 92. Providence, RI, USA: American Mathematical Soc., 1997.

[39] K. J. Worsley, S. Marrett, P. Neelin, A. C. Vandal, K. J. Friston, and A. C. Evans, "A unified statistical approach for determining significant signals in images of cerebral activation," *Human Brain Mapping*, vol. 4, no. 1, pp. 58–73, 1996.

[40] M. J. Jafri, G. D. Pearlson, M. Stevens, and V. D. Calhoun, "A method for functional network connectivity among spatially independent resting-state components in schizophrenia," *Neuroimage*, vol. 39, no. 4, pp. 1666–1681, Feb. 2008.

[41] J. Wang, X. Zuo, and Y. He, "Graph-based network analysis of resting-state functional MRI," *Frontiers Syst. Neurosci.*, vol. 4, p. 16, Jun. 2010.

[42] Z. Zhu, R. Wang, and F. Zhu, "The energy coding of a structural neural network based on the Hodgkin–Huxley model," *Frontiers Neurosci.*, vol. 12, p. 122, Mar. 2018.

[43] J. D. Power, D. A. Fair, B. L. Schlaggar, and S. E. Petersen, "The development of human functional brain networks," *Neuron*, vol. 67, no. 5, pp. 735–748, Sep. 2010.